Super scattering phenomenon in active spherical nanoparticles*

Chang-Yu Liu(刘昌宇)[1], Ya-Ming Xie(解亚明)[2,3], and Zhi-Guo Wang(王治国)[1,†]

[1] School of Physics Science and Engineering, Tongji University, Shanghai 200092, China
[2] Beijing Computational Science Research Center, Beijing 100193, China
[3] Department of Physics, University of Science and Technology of China, Hefei 230026, China

(Received 14 October 2016; revised manuscript received 5 February 2017; published online 20 April 2017)

Localized surface electromagnetic resonances in spherical nanoparticles with gain are investigated by using the Mie theory. Due to the coupling between the gain and resonances, super scattering phenomenon is raised and the total scattering efficiency is increased by over six orders of magnitude. The dual frequency resonance induced by the electric dipole term of the particle is observed. The distributions of electromagnetic field and the Poynting vector around nanoparticles are provided for better understanding different multipole resonances. Finally, the scattering properties of active spherical nanoparticles are investigated when the sizes of nanoparticles are beyond the quasi-static limit. It is noticed that more high-order multipole resonances can be excited with the increase of the radius. Besides, all resonances dominated by multipole magnetic terms can only appear in dielectric materials.

Keywords: super scattering, gain, plasmonic resonance, Mie theory

PACS: 78.67.–n, 42.70.–a, 42.25.Fx, 52.38.–r **DOI:** 10.1088/1674-1056/26/6/067803

1. Introduction

Surface plasmon resonance (SPR) is the resonant oscillation of conduction electrons at the interface between metal and dielectric at the frequency of incident radiation. Its characteristic of confining the electromagnetic fields to the interface bridges the gap between conventional optics and nano-optics. In nanoparticles, the induced SPR is confined in all three dimensions, which is known as localized surface plasmon resonance (LSPR). The research and cognition of surface plasmons[1–4] have proceeded for several decades and lots of applications of SPRs have been discovered in various nanostructures, such as biosensor,[5,6] waveguide,[6] and holography.[7] Meanwhile, the extinction and scattering technologies on a nanoscale are valuable to electromagnetic cloaking[8] and the manipulation of optical information transmission.

As is well known, energy loss is inevitable when an electromagnetic wave propagates in metallic material. Many different ways to mitigate loss and improve the performance of SPR structure have been proposed.[9] One effective strategy to overcome the energy dissipation is to introduce suitable gain into lossy material,[10–13] which can compensate for the loss to achieve nonloss, even optical amplification. The commonly used gain materials are comprised of fluorescent molecules[14] and quantum dots.[15,16] Gain has been used as a stimulated source to realize surface plasmon amplification by stimulated emission of radiation (Spaser).[17] Theoretical and experimental demonstrations[18] of loss compensation and amplification in an optical negative-index active metamaterial have been reported by Wustener *et al.*[19] and Xiao[20] *et al.* Furthermore, the coupling between the gain and SPRs would be mutually stimulated to generate extraordinary optical amplification. It was reported that the gain-assisted core-shell structure can achieve low-threshold surface plasmon amplification.[21–23] In addition, the anomalous forward scattering of nanoparticles was achieved with specific gain, which is attributed to the excitation of a magnetic or electric dipole resonance.[24] Due to the fact that the germanium-based materials are widely applied to advanced electronic devices, the absorption spectra and optical gain of Ge have also been studied in detail.[25,26] At present the mainly theoretical studies about the gain model are confined to two methods: one is to add the gain into a non-dispersive dielectric material; another is to use the Lorentzian line shape model for describing the gain.[11,13] However, we put forward the modified Drude model to describe the gain in active spherical nanoparticles, and the analysis of resonances caused by electric and magnetic multipole modes can be more exhaustive.

In this paper, the localized surface electromagnetic resonances in a dispersive homogenous spherical nanoparticle with gain are studied in theoretical analysis. The interaction between the gain and resonances is investigated as a function of the gain coefficient and the radius of the nanoparticle. Through introducing gain into the nanoparticle, the extinction characteristics of the particle indicate that it acts like a laser resonator and Spaser can be achieved at the critical point where the extinction efficiency is eliminated to zero. The utilization of suitable gain regarded as a stimulated pump source can amplify

*Project supported by the National Natural Science Foundation of China (Grant Nos. 11174222 and 91230203).
†Corresponding author. E-mail: zgwang@tongji.edu.cn
© 2017 Chinese Physical Society and IOP Publishing Ltd

the total scattering efficiency by over six orders of magnitude.

2. Theoretical model

Supposing that an active nonmagnetic dispersive spherical nanoparticle with radius R and permittivity $\varepsilon_{\rm p}$ is immersed in a vacuum, the dispersion relation of the particle is described by the Drude model,[27]

$$\varepsilon_{\rm p}(\omega) = \varepsilon_{\infty} - \frac{\omega_{\rm p}^2}{\omega(\omega + \gamma {\rm i})}. \tag{1}$$

Here, $\omega_{\rm p}$ and γ represent the plasma frequency and gain coefficient, γ takes negative value,[28] and ε_{∞} is the permittivity when ω verges to infinity. In this paper, the plasma frequency of silver is applied, which is $\omega_{\rm p} = 1.39 \times 10^{16}$ rad/s.[29]

The scattered field of a spherical nanoparticle can be expressed by the Mie scattering coefficients a_n and b_n, which can be determined by the boundary conditions at the surface of the particle. For each order n there are two distinct modes: coefficient a_n represents the transverse magnetic (TM) mode and coefficient b_n denotes the transverse electric (TE) mode. In some literature the TM mode is also known as electric term or E-wave, and similarly the TE mode is also called magnetic term or H-wave.[30] The total scattering ($Q_{\rm sca}$) and extinction ($Q_{\rm ext}$) efficiencies can be expressed in terms of these Mie coefficients as

$$Q_{\rm sca} = \frac{2}{x^2} \sum_{n=1}^{\infty} (2n+1)\left(|a_n|^2 + |b_n|^2\right), \tag{2}$$

$$Q_{\rm ext} = \frac{2}{x^2} \sum_{n=1}^{\infty} (2n+1) Re(a_n + b_n). \tag{3}$$

The absorption efficiency can be calculated from $Q_{\rm abs} = Q_{\rm ext} - Q_{\rm sca}$. Following the form of Bohern,[30] the Mie coefficients can be written as

$$a_n = \frac{\sqrt{\varepsilon}_{\rm p}\psi_n(mx)\psi_n'(x) - \psi_n(x)\psi_n'(mx)}{\sqrt{\varepsilon}_{\rm p}\psi_n(mx)\xi_n'(x) - \xi_n(x)\psi_n'(mx)}, \tag{4}$$

$$b_n = \frac{\psi_n(mx)\psi_n'(x) - \sqrt{\varepsilon}_{\rm p}\psi_n(x)\psi_n'(mx)}{\psi_n(mx)\xi_n'(x) - \sqrt{\varepsilon}_{\rm p}\xi_n(x)\psi_n'(mx)}. \tag{5}$$

Here, the radial functions ψ_n and ξ_n are respectively the Ricatti–Bessel and Hankel functions of size parameter $x = 2\pi R/\lambda$ and refractive index $m = \sqrt{\varepsilon}_{\rm p}$, and λ is the incident wavelength in a vacuum.

It can be derived from Eqs. (4) and (5) that for ordinary lossy and lossless materials, the real parts of the Mie coefficients are always positive. Thus the extinction efficiency can never be reduced to zero, which is a crucial condition in pursuing Spaser. When gain is introduced in material, the above-mentioned restriction can be broken, which gives the opportunity of achieving Spaser. Furthermore, it has been reported in Ref. [24] that super scattering will appear with introducing the specific gain, which can be attributed to the resonance caused by a particular multipole mode.

3. Results and discussion

Figure 1 shows the total scattering ($Q_{\rm sca}$), extinction ($Q_{\rm ext}$), and absorption ($Q_{\rm abs}$) efficiencies for spherical nanoparticles each as a function of $\omega/\omega_{\rm p}$ calculated by the Mie theory. Here the radius of the nanoparticle is 65.1 nm and the parameter used in the Drude model is $\varepsilon_{\infty} = 1$.

The $Q_{\rm ext}$, $Q_{\rm sca}$, and $Q_{\rm abs}$ of a lossless ($\gamma/\omega_{\rm p} = 0$) nanoparticle are provided in Fig. 1(b). The complete overlap between $Q_{\rm sca}$ and $Q_{\rm ext}$ demonstrates that the incident wave is totally scattered into the vacuum and no energy is absorbed by the particle. There are four plasmonic resonances shown in Fig. 1(b), which are caused by the electric dipole ($\omega/\omega_{\rm p}$= 0.33), quadrupole ($\omega/\omega_{\rm p}$= 0.49), octupole ($\omega/\omega_{\rm p}$= 0.575), and hexadecapole ($\omega/\omega_{\rm p}$= 0.62) modes, respectively. According to the analysis in Ref. [31], the resonances caused by higher order modes are more susceptible to the introduction of dissipation than by lower order ones. Thus in Fig. 1(a), due to the use of lossy materials, it is observed that the electric hexadecapole resonance vanishes. In addition, in Fig. 1(a) the magnitudes of the electric dipole, quadrupole and octupole resonances are reduced and their linewidths are broadened, when compared with those in Fig. 1(b).

In Fig. 1(c), the optical cross sections of an active ($\gamma/\omega_{\rm p} = -0.05$) spherical nanoparticle are provided. The negative $Q_{\rm abs}$ implies that the gain serves as a stimulated source which can eradiate energy into surrounding medium. Like the situation in Fig. 1(a), it is observed that in Fig. 1(c) the resonance induced by the electric hexadecapole mode also disappears. When $\gamma/\omega_{\rm p}$ further decreases to -0.135, it is shown in Fig. 1(d) that a strong plasmonic resonance is stimulated at $\omega/\omega_{\rm p} = 0.49$, which is caused by the electric quadrupole mode. The maximum magnitudes of $Q_{\rm sca}$ and $Q_{\rm abs}$ reach about 2.2×10^6, and it is clearly observed from the inset of Fig. 1(d) that $Q_{\rm ext}$ is reduced to zero due to the complete offset between $Q_{\rm sca}$ and $Q_{\rm abs}$. Besides, the linewidths of $Q_{\rm sca}$ and $Q_{\rm abs}$ are extremely narrow. All these phenomena demonstrate that at this resonant position the nanoparticle acts like a nanolaser resonator.[32,33] The value of $\gamma/\omega_{\rm p}$ at the critical point where $Q_{\rm ext} = 0$ is called the gain threshold in nanolaser. As the gain is increased to the critical point, it can serve as excitation sources to completely compensate for the energy dissipation caused by scattering.

To analyze the continual change of total scattering efficiency with the variation of gain, the values of $Q_{\rm sca}$ of two nanospheres with the same radius R while different values of permittivity ε_{∞} are provided in Fig. 2, and the dominant multipole mode in each resonance is also investigated. Figure 2(a) illustrates the two-dimensional (2D) pseudocolor plot of $Q_{\rm sca}$ as a function of $\omega/\omega_{\rm p}$ and $\gamma/\omega_{\rm p}$ for a spherical nanoparticle with $R = 65.1$ nm and $\varepsilon_{\infty} = 1$. Through introducing gain

in material, it is noticed in Fig. 2(a) that Q_{sca} experiences a remarkable enhancement and the maximum of Q_{sca} can exceed 10^6. In addition, the induced plasmonic resonances in nanospheres can also react with the gain to stimulate more emissions. Finally a positive interaction between the plasmonic resonances and gain is established, which will lead to the appearance of super scattering phenomenon. The dashed-dotted line (denoting $\mathrm{Re}(\varepsilon_p) = 0$) in Fig. 2(a) divides the plot into two parts: in the left part the real parts of permittivities are negative, while in the right part they are positive. As shown in the left region ($\mathrm{Re}(\varepsilon_p) < 0$) of Fig. 2(a), when γ/ω_p is increased from -1.0 to 0, besides electric dipole resonance (maximum at $\gamma/\omega_p = -0.66$ and $\omega/\omega_p = 0.39$), more higher-order resonances, such as electric quadrupole (maximum at $\gamma/\omega_p = -0.13$ and $\omega/\omega_p = 0.49$) and octupole (maximum at $\gamma/\omega_p = -0.02$ and $\omega/\omega_p = 0.57$) resonances, can be excited in the spectrum of Q_{sca}. Besides, the LSPRs caused by electric multipole terms show blue-shift with the decrease of γ/ω_p. However, in the right region ($\mathrm{Re}(\varepsilon_p) < 0$) of Fig. 2(a) only resonance contributed by the electric dipole term is observed. The high and low frequency electric dipole resonances constitute the dual frequency resonance phenomenon. It is noticed in Fig. 2(a) that the high frequency electric dipole resonance in the right part is weaker than the low frequency one in the left part. This is because the low frequency electric dipole resonance is excited with metallic material ($\mathrm{Re}(\varepsilon_p) < 0$), while the high frequency one is stimulated in dielectric material ($\mathrm{Re}(\varepsilon_p) > 0$).

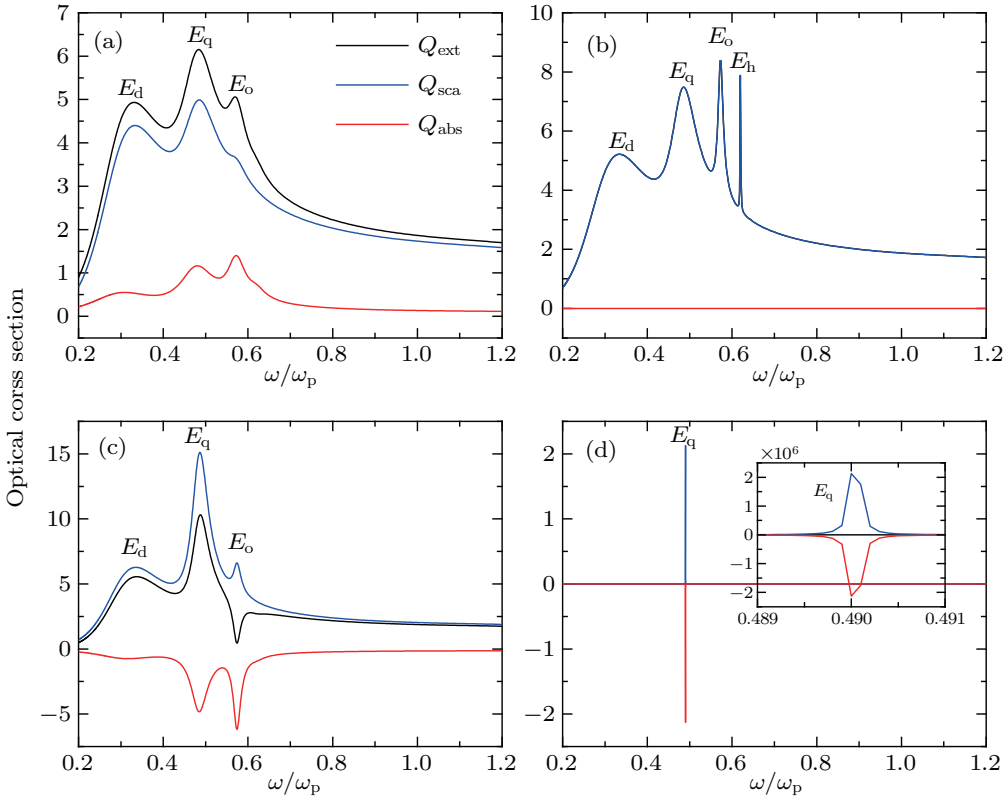


Fig. 1. (color online) ((a)–(d)) The optical cross sections each as a function of ω/ω_p for spherical nanoparticles with $\gamma/\omega_p = 0.05, 0, -0.05$, and -0.135, respectively. Here the radius of the particle is $R = 65.1$ nm and the permittivity used in the Drude model is $\varepsilon_\infty = 1$. The inset in panel (d) shows $Q_{ext} = 0$ at the critical point. Abbreviations for resonances: E_d, electric dipole; E_q, electric quadrupole; E_o, electric octupole; E_h, electric hexadecapole.

The upper plot in Fig. 2(b) gives the optical cross section for a spherical nanoparticle with $R = 65.1$ nm, $\varepsilon_\infty = 1$ and $\gamma/\omega_p = -0.8$, which corresponds to the horizontal dashed line in Fig. 2(a). The dual frequency resonance phenomenon is clearly observed. To demonstrate the dominant multipole mode in each resonance, the real and imaginary parts of the first three electric terms (a_1, a_2, and a_3) are indicated by the lower plot of Fig. 2(b). It is noticed that in the whole frequency range the magnitudes of electric quadrupole and octupole terms are much smaller than that of electric dipole term, which confirms the results obtained in Fig. 2(a).

Figure 2(c) provides Q_{sca} as a function of ω/ω_p and γ/ω_p for a spherical nanoparticle with $R = 65.1$ nm and $\varepsilon_\infty = 3$. Unlike the situation in Fig. 2(a), where the dual frequency resonance dominated by the electric dipole term is not remarkable, one can distinctly observe the super scattering and enhanced resonances caused by the magnetic dipole, quadrupole and octupole terms. The resonances caused by the three magnetic multipole modes show red-shift with the decrease of γ/ω_p. Like the situation in Fig. 2(a), in the left part of the dashed-dotted line the real parts of permittivities are negative, while in the right part they are positive. In the past few

years, researchers have shown experimentally[34] that dielectric ($\mathrm{Re}(\varepsilon_\mathrm{p}) > 0$) nanoparticles with moderate permittivity simultaneously present strong magnetic and electric dipole resonances, while metallic ($\mathrm{Re}(\varepsilon_\mathrm{p}) < 0$) nanoparticles can only support electric dipole resonances. Thus it is found that no resonance resulting from multipole magnetic terms can appear in the left region ($\mathrm{Re}(\varepsilon_\mathrm{p}) < 0$) of Fig. 2(c).

To illustrate the conclusions obtained from Fig. 2(c), the optical cross sections and the real and imaginary parts of the first three magnetic terms (b_1, b_2, and b_3) each as a function of ω/ω_p are given in Fig. 2(d) for a spherical nanoparticle with $R = 65.1$ nm, $\varepsilon_\infty = 3$ and $\gamma/\omega_\mathrm{p} = -0.8$, which corresponds to the horizontal dashed line in Fig. 2(c). It is observed that the three resonances in the upper plot of Fig. 2(d) stem from the magnetic dipole, quadrupole and octupole terms, respectively, and no resonance caused by electric multipole terms appears.

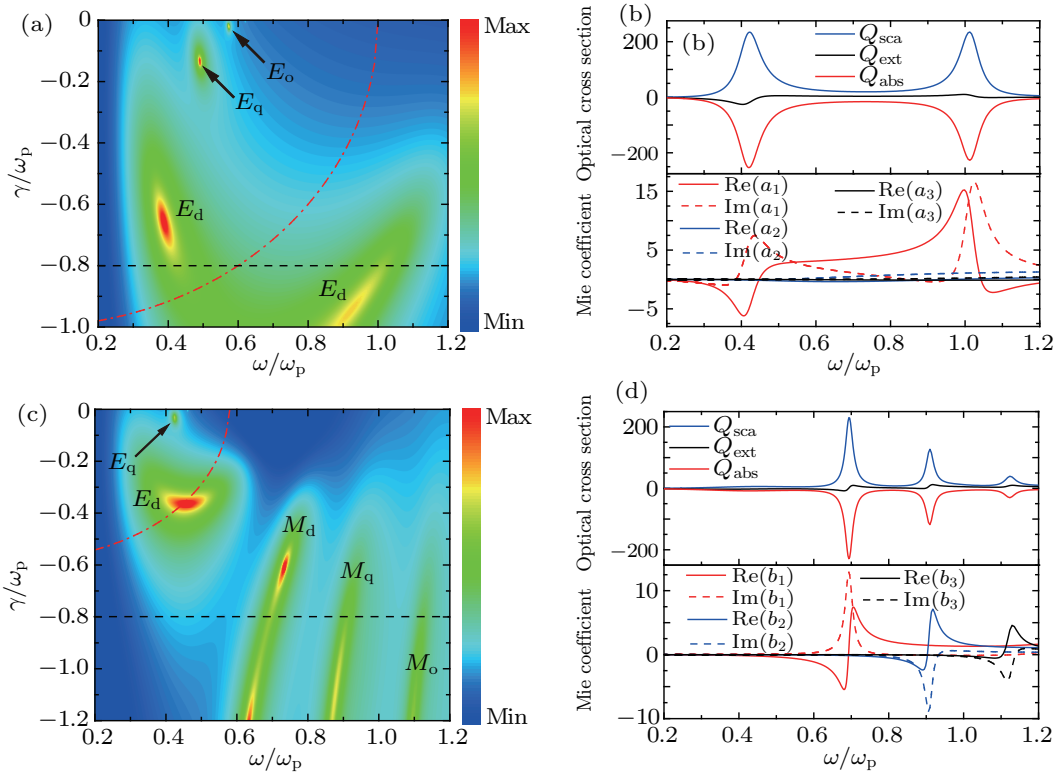


Fig. 2. (color online) 2D pseudocolor plots of Q_sca (logarithm–ic scale) for spherical nanoparticles as functions of ω/ω_p and γ/ω_p with (a) $\varepsilon_\infty = 1$ and (c) $\varepsilon_\infty = 3$. Here the radius of particle is $R = 65.1$ nm. The dashed-dotted lines in panels (a) and (c) denote these points where the real parts of permittivities are zero. The optical cross sections and Mie coefficients each as a function of ω/ω_p for spherical nanoparticles with (b) $\varepsilon_\infty = 1$, $\gamma/\omega_\mathrm{p} = -0.8$, and (d) $\varepsilon_\infty = 3$, $\gamma/\omega_\mathrm{p} = -0.8$. Abbreviations for resonances: M_d, magnetic dipole; M_q, magnetic quadrupole; M_o, magnetic octupole.

For better understanding these resonances resulting from multipole terms, the distributions of scattered electric and magnetic field intensities are shown in Fig. 3. The propagation direction of incident wave is in the $+Z$ axis direction and the electric vector polarizes along the X axis. Figure 3(a) displays the scattered electric field intensity distribution for a spherical nanoparticle with radius $R = 65.1$ nm and permittivity $\varepsilon_\mathrm{p} = -0.7 - 2.9\mathrm{i}$ at incident wavelength $\lambda = 348.7$ nm. The parameters used here are obtained from the maximum point of electric dipole term ($\omega/\omega_\mathrm{p} = 0.39$ and $\gamma/\omega_\mathrm{p} = -0.66$) in Fig. 2(a), thus the scattering of the active nanoparticle is dominated by the electric dipole mode. It is noticed that here the electric field distribution is obviously caused by the induced electric dipole moment in the particle. The scattered electric field is enhanced and reaches maxima on the surface of the particle along the polarization direction of incident electric vector.

Figure 3(b) shows the projections of the Poynting vector $\langle \boldsymbol{S} \rangle = 1/2\mathrm{Re}(\boldsymbol{E} \times \boldsymbol{H}^*)$ of the scattered field on X–Z plane for the same nanoparticle shown in Fig. 3(a). It is apparent that energy outflows from the center of the particle to surrounding medium along the $\pm Z$ axis and reaches maxima on the surface of the particle. The effluent energy partly originates from the gain in material which causes Spaser.

Figure 3(c) shows the distribution of scattered electric field intensity around an active spherical nanoparticle with radius $R = 65.1$ nm and permittivity $\varepsilon_\mathrm{p} = -2.9 - \mathrm{i}$ at incident wavelength $\lambda = 276.5$ nm. Here the parameters correspond to the maximum point of electric quadrupole term ($\omega/\omega_\mathrm{p} = 0.49$ and $\gamma/\omega_\mathrm{p} = -0.13$) in Fig. 2(a). The situation of incident field is just the same as that in Fig. 3(a). Along the surface of the nanoparticle there exist four areas where the scattered electric field intensity shows a relative maximum, which corresponds to the characteristic of the electric field distribution caused by an induced electric quadrupole moment. The corresponding

projections of the Poynting vector are plotted on X–Z plane in Fig. 3(d). It is also found that the projections of the Poynting vector in four directions are larger than those in other directions on the surface of the particle.

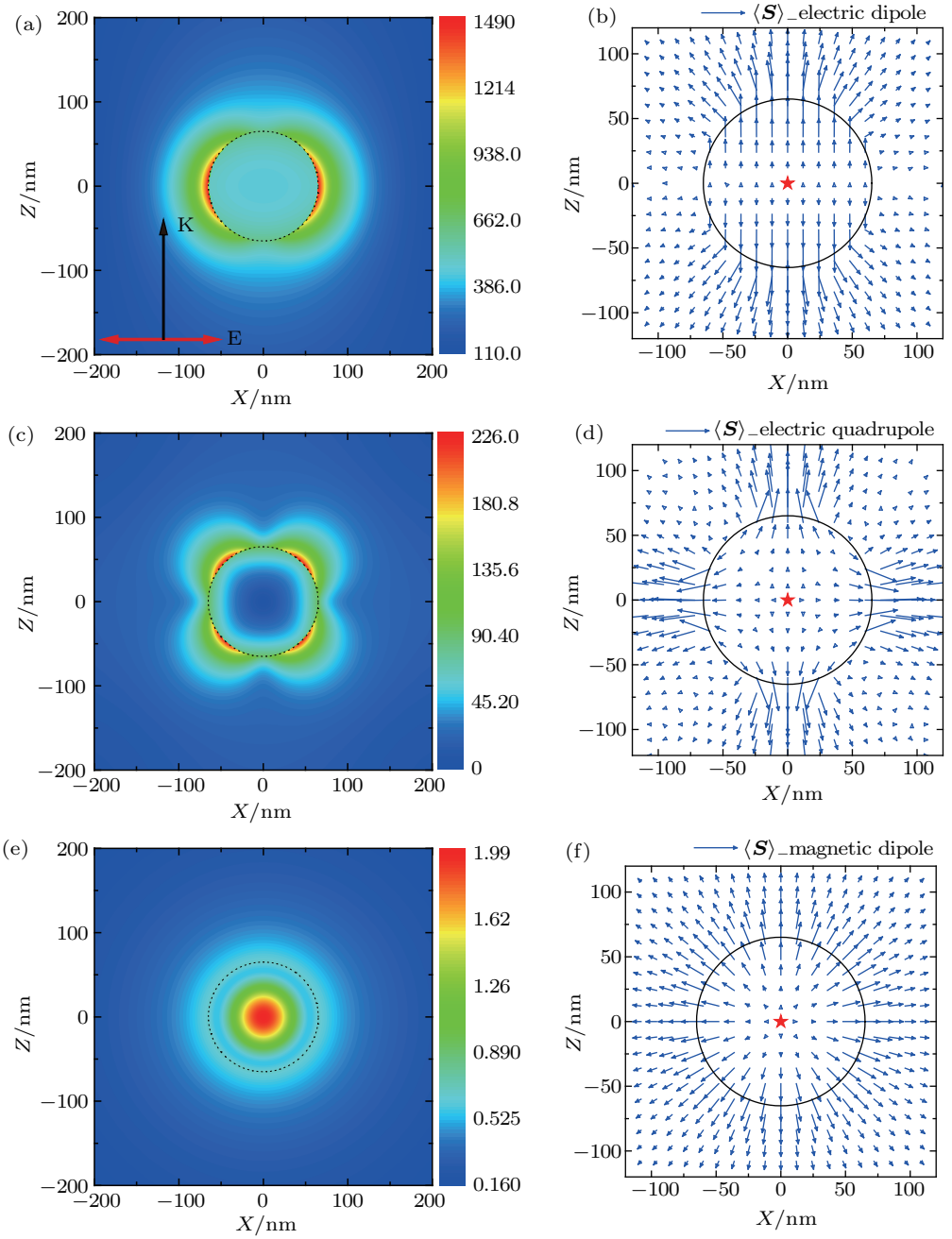


Fig. 3. (color online) Scattered electric field intensity distributions of an active spherical nanoparticle with $R = 65.1$ nm at (a) $\varepsilon_p = -0.7 - 2.9\mathrm{i}$ and $\lambda = 348.7$ nm and (c) $\varepsilon_p = -2.9 - \mathrm{i}$ and $\lambda = 276.5$ nm. The scattered magnetic field intensity distribution around an active spherical nanoparticle with $R = 65.1$ nm at (e) $\varepsilon_p = 1.9 - 0.91\mathrm{i}$ and $\lambda = 184.7$ nm. Panels (b), (d) and (f) show the corresponding projections of the Poynting vector on X–Z plane of panels (a), (c), and (e), respectively. The "Red Star" represents the source of the Poynting vector.

The scattered magnetic field intensity distribution around a spherical nanoparticle is provided in Fig. 3(e). Here the radius and permittivity of the particle are $R = 65.1$ nm and $\varepsilon_p = 1.9 - 0.91\mathrm{i}$, and the incident wavelength is $\lambda = 184.7$ nm. These parameters are derived from the maximum point of magnetic dipole term ($\omega/\omega_p = 0.73$ and $\gamma/\omega_p = -0.6$) in Fig. 2(c), thus the resonance in the active nanoparticle is triggered by the magnetic dipole mode. In Fig. 3(e) one can observe a typical magnetic field intensity distribution caused by a magnetic dipole. The magnitude of magnetic field reaches a maximum value in the center of the particle and is rapidly reduced with the increase of radius. The corresponding projections of the Poynting vector on X–Z plane are shown in Fig. 3(f). It is clear that the energy goes out radially from the center of the particle to surrounding medium and the projection of the Poynting vector reaches maxima on the surface of the particle.

Size parameter x has a profound effect on scattering prop-

erties of spherical nanoparticles. In quasi-static limit ($x \ll 1$), optical cross sections are dominated by the dipole terms and the incident wave can be considered as a static field. When the size of nanoparticle is beyond the quasi-static limit, phase retardation effect is not negligible, which can cause the electric and magnetic multipole modes to occur.

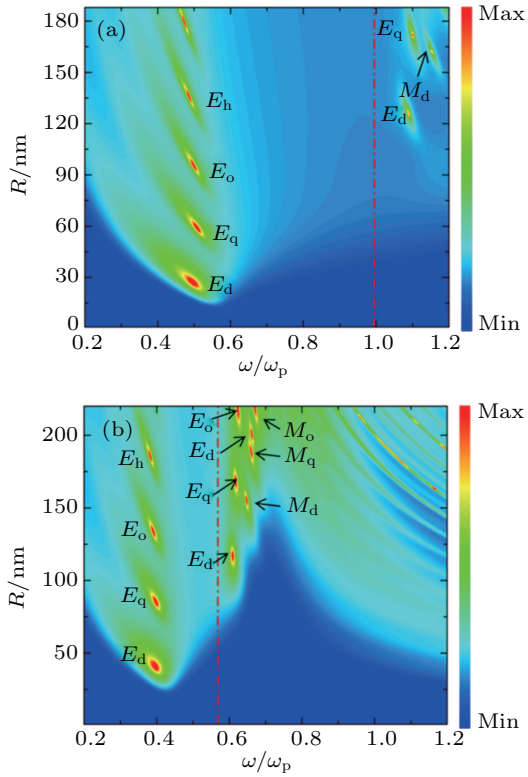


Fig. 4. (color online) 2D pseudocolor plots of Q_{sca} (logarithmic scale) each as a function of ω/ω_p and radius R for spherical nanoparticles with (a) $\varepsilon_\infty = 1$ and (b) $\varepsilon_\infty = 3$. Here the gain coefficient is $\gamma/\omega_p = -0.1$. The dashed–dotted lines in panels (a) and (b) denote these points where the real parts of permittivities are zero.

Resonances contributed by multipole terms can be excited by increasing the radius of the active nanoparticle. Figure 4(a) presents the 2D pseudocolor plot of Q_{sca} for a spherical nanoparticle with $\varepsilon_\infty = 1$ and $\gamma/\omega_p = -0.1$ as a function of ω/ω_p and R. The dashed-dotted lines in Figs. 4(a) and 4(b) have the same meaning (denoting $\mathrm{Re}(\varepsilon_p) = 0$) as those in Figs. 2(a) and 2(c), and the real parts of permittivities in the left and right parts of the dashed-dotted line are negative and positive, respectively. As discussed above, in the left region ($\mathrm{Re}(\varepsilon_p) < 0$) of Fig. 4(a) all resonances are caused by electric multipole terms, and resonances resulting from magnetic multipole terms can only appear in the right region ($\mathrm{Re}(\varepsilon_p) > 0$). It is noticed in the left region of Fig. 4(a) that with the increase of the radius R, the dominant contribution in the scattering spectrum will gradually change from the electric dipole term (maximum at $R = 25$ nm and $\omega/\omega_p = 0.5$) to other higher order electric terms, and the maxima of these resonances occur at almost the same frequency ($\omega/\omega_p = 0.5$). Besides, red-shift is observed for each plasmonic resonance caused by electric multipole terms with increasing the radius. In the right region of Fig. 4(a), there are two resonances dominated by the electric dipole ($R = 126$ nm) and quadrupole ($R = 173$ nm) terms occurring at about $\omega/\omega_p = 1.1$. Meanwhile a resonance contributed by the magnetic dipole term is stimulated at $R = 163$ nm and $\omega/\omega_p = 1.15$.

Figure 4(b) shows the 2D pseudocolor plot of Q_{sca} similar to the situation in Fig. 4(a) but with $\varepsilon_\infty = 3$. In the left region of Fig. 4(b) the maxima of the plasmonic resonances dominated by electric multipole terms appear at $\omega/\omega_p = 0.4$. In addition, resonances resulting from electric multipole terms can also occur at about $\omega/\omega_p = 0.62$ in the right region of Fig. 4(b). It is noticed that some resonances dominated by magnetic multipole terms are stimulated at $\omega/\omega_p = 0.66$ in the right region of Fig. 4(b), such as magnetic dipole (at $R = 152$ nm), quadrupole (at $R = 188.5$ nm), and octupole (at $R = 220$ nm) terms. Thus with the increase of ε_∞, more resonances dominated by magnetic multipole terms can be excited.

4. Conclusions

In this work, the scattering properties of dispersive spherical nanoparticles with different gains are carefully analyzed by using the Mie theory. The total scattering efficiency is amplified by over six orders of magnitude with suitable gain in material. The nanoparticles with gain can be regarded as nanolaser resonators, which can achieve optical amplification even Spaser. Mutual stimulation between the localized surface electromagnetic resonances and gain will induce super scattering. Dual frequency resonance caused by the electric dipole mode is observed. The high frequency resonance is excited with dielectric ($\mathrm{Re}(\varepsilon_p) > 0$) materials, while the low frequency one is stimulated in metallic ($\mathrm{Re}(\varepsilon_p) < 0$) materials. Simulated distributions of the scattered electric and magnetic field intensities at different multipole resonance peaks are presented, and the corresponding patterns of the Poynting vector are also provided for further illustrating the energy transfer situation around nanoparticles. With the increase of the radius of nanoparticles, resonances generated by high ($n \geq 2$) electric and magnetic multipole terms are also observed, which is attributed to the phase retardation effect. All resonances dominated by magnetic multipole terms can only appear in dielectric materials. The results in this work show that it would be an efficient way to stimulate the localized surface electromagnetic resonance contributed by any electric or magnetic multipole mode in active spherical nanoparticles with the specific combination of the permittivity and radius.

References

[1] Barnes W L, Dereux A and Ebbesen T W 2003 *Nature* **424** 824
[2] Avrutsky I 2004 *Phys. Rev. B* **70** 155416
[3] Li Z Y and Xia Y 2010 *Nano. Lett.* **10** 243

[4] Ma Y W, Wu Z W, Zhang L H, Liu W F and Zhang J 2015 *Chin. Phys. Lett.* **32** 094202
[5] Liedberg B, Nylander C and Lunström I 1983 *Sensors & Actuators* **4** 299
[6] Homola J, Yee S S and Gauglitz G 1999 *Sensors & Actuators B- Chemical* **54** 3
[7] Ozaki M, Kato J and Kawata S 2011 *Science* **332** 218
[8] Schurig D, Mock J J, Justice B J, Cummer S A, Pendry J B, Starr A F and Smith D R 2006 *Science* **314** 977
[9] Khurgin J B 2015 *Nat. Nanotechnol.* **10** 2
[10] De Luca A, Ferrie M, Ravaine S, La Deda M, Infusino M, Rashed A R, Veltri A, Aradian A, Scaramuzza N and Strangi G 2012 *J. Mater. Chem.* **22** 8846
[11] Veltri A and Aradian A 2012 *Phys. Rev. B* **85** 115429
[12] Zhu W R, Rukhlenko I D and Premaratne M 2012 *Appl. Phys. Lett.* **101** 031907
[13] Wu D J, Wu X W, Cheng Y, Jin B B and Liu X J 2015 *Appl. Phys. Lett.* **107** 191909
[14] Gather M C, Meerholz K, Danz N and Leosson K 2010 *Nat. Photon.* **4** 457
[15] Alivisatos A P 1996 *Science* **271** 933
[16] Klimov V I, Mikhailovsky A A, Xu S, Malko A, Hollingsworth J A, Leatherdale C A, Eisler H and Bawendi M G 2000 *Science* **290** 314
[17] Stockman M I 2008 *Nat. Photon.* **2** 327
[18] Hess O, Pendry J B, Maier S A, Oulton R F, Hamm J M and Tsakmakidis K L 2012 *Nat. Mater.* **11** 573
[19] Wuestner S, Pusch A, Tsakmakidis K L, Hamm J M and Hess O 2010 *Phys. Rev. Lett.* **105** 127401
[20] Xiao S, Drachev V P, Kildishev A V, Ni X, Chettiar U K, Yuan H K and Shalaev V M 2010 *Nature* **466** 735
[21] Ding P, He J N, Wang J Q, Fan C Z, Cai G W and Liang E J 2013 *J. Opt.* **15** 105001
[22] Tao Y F, Guo Z Y, Sun Y X, Shen F, Mao X Q, Wang W, Li Y, Liu Y, Wang X S and Qu S L 2015 *Opt. Commun.* **355** 580
[23] Zhang H P, Zhou J, Zou W B and He M 2012 *J. Appl. Phys.* **112** 074309
[24] Xie Y M, Tan W and Wang Z G 2015 *Opt. Express* **23** 2091
[25] Liu Z, He C, Zhang D L, Li C B, Xue C L, Zuo Y H and Cheng B W 2016 *Chin. Phys. B* **25** 057804
[26] Liu J F, Sun X C, Kimerling L C and Michel J 2009 *Opt. Lett.* **34** 1738
[27] Ordal M A, Bell R J, Alexander R W, Long L L and Querry M R 1985 *Appl. Opt.* **24** 4493
[28] Leonhardt U and Philbin T G 2007 *New J. Phys.* **9** 254
[29] Johnson P B and Christy R W 1972 *Phys. Rev. B* **6** 4370
[30] Bohren C F and Huffman D R 1998 *Absorption and Scattering of Light by Small Particles* (New York: Wiley) pp. 97–102
[31] Tribelsky M I and Luk'yanchuk B S 2006 *Phys. Rev. Lett.* **97** 263902
[32] Plum E, Fedotov V A, Kuo P, Tsai D P and Zheludev N I 2009 *Opt. Express* **17** 8548
[33] Stockman M I 2010 *J. Opt.* **12** 024004
[34] Evlyukhin A B, Novikov S M, Zywietz U, Eriksen R L, Reinhardt C, Bozhevolnyi S I and Chichkov B N 2012 *Nano Lett.* **12** 3749